

Multigrid preconditioning for efficient solution of the 3D Laplace problem for wave-body interaction

Harry B. Bingham*, Allan P. Engsig-Karup and Ole Lindberg†
 Technical University of Denmark,
 2800 Lyngby, Denmark
 (hbb,apek)@mek.dtu.dk, lindberg.ole@gmail.com

At the 22nd workshop in Croatia, we presented some preliminary three-dimensional (3D) results using a flexible-order finite difference based solution of the exact Laplace problem for nonlinear water waves and their interaction with fixed and floating structures [1]. The method is presented in detail in [2], including a stability and accuracy analysis and some results in two-dimensions (2D). In this abstract we describe a special treatment of the boundary conditions along solid boundaries which is necessary to obtain robust solutions, particularly when using multigrid preconditioning. With multigrid preconditioning, we demonstrate an optimal scaling of the overall solution effort, *i.e.* directly with n the total number of grid points. Full details of this and other aspects of the 3D solution will appear in [4].

To summarize the method, consider the exact potential flow problem in a Cartesian coordinate system with origin on the still water plane and the z -axis pointing vertically upwards; $\mathbf{x} = [x, y]$ is a horizontal vector and t is time. The fluid domain is bounded by the sea bottom at $z = -h(\mathbf{x})$, the free-surface at $z = \eta(\mathbf{x}, t)$, and a horizontal enclosing boundary S_b which may include fixed and/or floating structures. The free surface boundary conditions are expressed in terms of the velocity potential and the vertical velocity evaluated directly on the free-surface: $\tilde{\phi} = \phi(\mathbf{x}, \eta, t)$, and $\tilde{w} = \left. \frac{\partial \phi}{\partial z} \right|_{z=\eta}$

$$\eta_t = -\nabla \eta \cdot \nabla \tilde{\phi} + \tilde{w}(1 + \nabla \eta \cdot \nabla \eta) \quad (1a)$$

$$\tilde{\phi}_t = -g\eta - \frac{1}{2}\nabla \tilde{\phi} \cdot \nabla \tilde{\phi} + \frac{1}{2}\tilde{w}^2(1 + \nabla \eta \cdot \nabla \eta). \quad (1b)$$

Here $\nabla = [\partial/\partial x, \partial/\partial y]$ is the horizontal gradient operator, g the gravitational acceleration and partial differentiation is indicated when the independent variables appear as subscripts. These provide evolution equations for η and $\tilde{\phi}$ to be integrated forward in time from initial conditions, which is done using the classical explicit fourth-order Runge-Kutta method. To obtain the vertical component of velocity \tilde{w} from the known η and $\tilde{\phi}$, requires satisfying the Laplace equation throughout the fluid volume along with the solid boundary conditions:

$$\nabla^2 \phi + \phi_{zz} = 0, \quad -h < z < \eta \quad (2a)$$

$$\phi_z + \nabla h \cdot \nabla \phi = 0, \quad z = -h. \quad (2b)$$

$$\mathbf{n} \cdot (\nabla \phi, \phi_z) = V_n \quad \text{on } S_b \quad (2c)$$

where V_n is the normal velocity of the horizontal fluid boundary S_b with normal vector \mathbf{n} .

To solve this problem we apply a coordinate transformation which maps the irregularly shaped physical domain to a cuboid computational domain. One arbitrarily spaced set

*This work is made possible by the Danish Research Council for Technology and Production grant no. 274-06-0030, with supercomputing resources made available by the Danish Center for Super Computing.

†Now at DHI - Water & Environment, 2970 Hørsholm, Denmark

of grid coordinates is then taken along each computational direction, and arbitrary-order finite difference schemes are developed to express all first and second partial derivatives. The Laplace problem in this boundary-fitted, non-orthogonal coordinate system is more complicated, including both first- and cross-derivatives as well as derivatives of the transformation, but the essential character is unchanged as is the basic structure of the resultant linear system of equations

$$\mathbf{A}\mathbf{p} = \mathbf{b}. \quad (3)$$

The application of this general idea is widespread, and its use for the simulation of unsteady free-surface flows goes back at least to [5, 3]. The attraction of this approach lies in the time invariance of the computational operators (no re-gridding is required) and in the relative ease of obtaining a high-order representation of the solution including complex fixed and moving boundaries. The new aspects of the present work have to do with development of robust discretization strategies (in particular along solid boundaries) and efficient solution of (3) to obtain optimal scaling of both RAM memory use and CPU time. Our solution is also quite flexible, allowing adaptation of both the grid and the order of accuracy of the discrete derivative operators.

To solve (3) we employ the GMRES (Generalized Minimal RESidual) Krylov subspace iterative method with a linear extrapolation from the two previous time solutions as the initial guess. The performance of GMRES is sensitive to the preconditioning, and for this purpose we use the linearized version of the matrix discretized to second-order accuracy \mathbf{M} . Preconditioning on the left, (3) becomes (symbolically) $\mathbf{M}^{-1}(\mathbf{A}\mathbf{p}) = \mathbf{M}^{-1}\mathbf{b}$. A preconditioning operation thus requires solving a linear system of the form $\mathbf{M}\mathbf{q} = \mathbf{s}$. In practice, the preconditioning operation is taken to be one multigrid V-cycle with an initial guess of $\mathbf{q} = 0$. Although we do not claim that this is *the* optimum strategy, it performs quite well giving a reasonably even distribution of computational effort between the matrix-vector product and the preconditioning operation.

Figure 1 plots with increasing n both the average CPU time per iteration and the total RAM memory required to solve a mildly nonlinear standing wave test problem which has been chosen to exercise all the features of the model. The plots compare the behavior of a

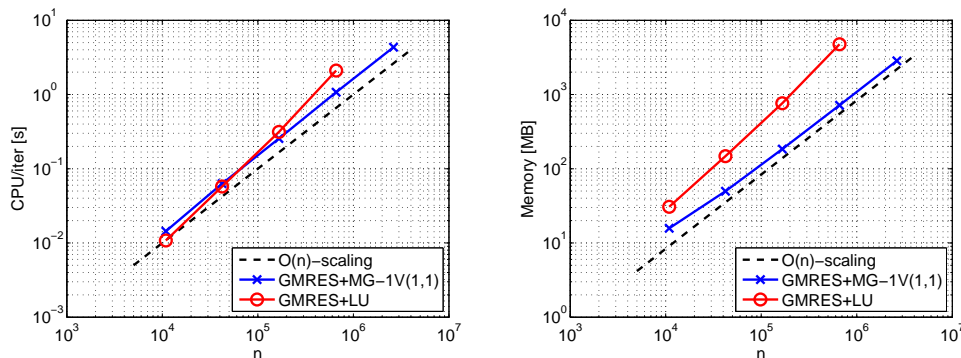


Figure 1: Scaling of computational effort, and RAM memory use.

multigrid and a direct solution of the preconditioning problem. Using multigrid clearly provides optimal scaling of both memory use and computational effort while the direct strategy scales super-linearly with increasing problem size. The code is written in FORTRAN90/95 and these calculations were made on one AMD Opteron node with two dual-core processors running at 2.6 GHz.

The key to a robust numerical solution to the problem as described above lies in the imposition of the boundary conditions along the solid boundaries. In the context of a collocated finite difference scheme with both η and ϕ defined at the same set of grid points, it is natural to define a grid which includes points directly on the solid wall boundaries. The degrees of freedom associated with these boundary points are then used to impose the no-flux boundary condition by writing off-centered finite difference schemes and replacing the Laplace equation at those points with the boundary condition. We will refer to this strategy as “BC”. An alternative strategy is to imagine a set of “ghost points” external to the fluid boundary and write finite difference schemes which include these points to impose the boundary condition. The resultant boundary equations can then be solved explicitly to express the ghost point values in terms of the internal grid point values. Finally, the ghost point contributions are eliminated from the discrete Laplace equation applied at the boundary. We will refer to this strategy as “BC+LAPLACE”.

Figure 2 shows the result of a discrete linear stability analysis of the two strategies applied to a particular discretization on a flat bottom (see [4] for the details). Here $|\lambda|_{max}$

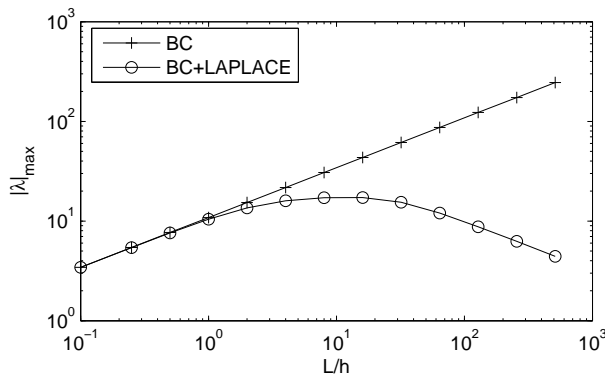


Figure 2: Maximum eigenvalues of the Jacobian matrix for the method under the two boundary discretization schemes plotted vs. relative water depth.

is the maximum absolute value of the eigenvalues of the Jacobian matrix for the linearized system. This plot shows that the two strategies have the same stability requirements in deep water but they are dramatically different in shallow water. The eigenvalues of the discrete system are very nearly pure imaginary, so stability under R-K(4,4) time-stepping is governed by $\Delta t |\lambda|_{max} \leq 2\sqrt{2}$, (*i.e.* the extent of the imaginary axis included by the R-K(4,4) stability region.) For example when $h = L/100$, strategy BC will require a time step which is approximately ten times smaller than the one required for $h = L$. On the other hand, for strategy BC+LAPLACE the stability requirements are largely independent of relative water depth.

Only the treatment of the horizontal boundary conditions influences this stability analysis and the picture is the same whether the bottom boundary condition is implemented using strategy BC or BC+LAPLACE. Gauss-Seidel iteration (and hence multigrid) on the other hand, turns out to be sensitive to the treatment of the bottom boundary condition. The essential difference between the two strategies here is in the diagonal dominance properties of the resultant matrix. For strategy BC+LAPLACE, the boundary point equations are the Laplace equation with the boundary condition built in and hence of essentially the same character as the interior point equations. In this case, the resultant matrix is mildly diagonally dominant in the limit of a linear problem on a constant depth. Gauss-Seidel iteration is thus guaranteed to be convergent in this limit. Although a non-zero bottom slope

will work to reduce the diagonal dominance in the system, we have so far not found any divergent examples regardless of the physical parameters and/or the grid anisotropy. On the other hand, the exchange of the Laplace equation for the bottom boundary condition inherent in strategy BC apparently reduces the diagonal dominance of the matrix to such a degree that Gauss-Seidel iteration becomes divergent, even at relatively small values of bottom slope and/or grid anisotropy.

Figure 3 shows a sample calculation for monochromatic waves shoaling on a circular shoal and compares the result to experimental measurements of [6]. At this point we have validated the accuracy and efficiency of the method on simple geometries, the next step will be to apply transformations along the other coordinates to treat more interesting structures.

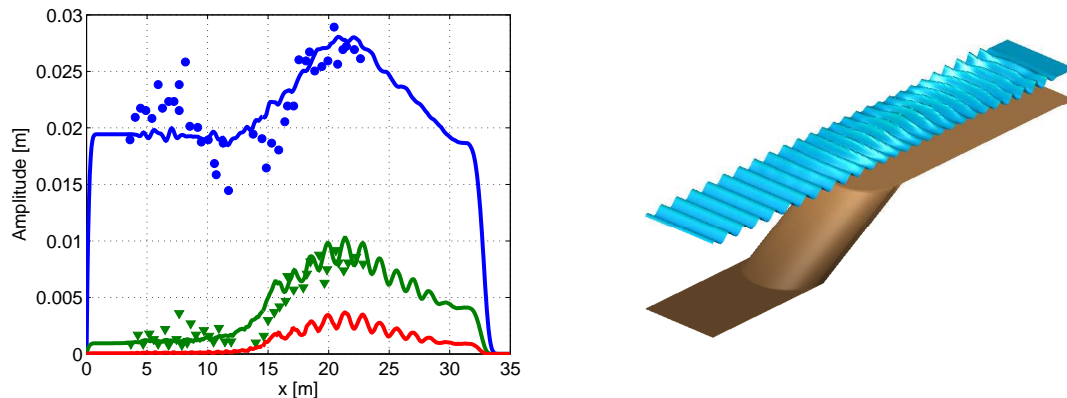


Figure 3: Harmonic analysis of measured and computed results for the experiments of Whalin at wave period $T=1s$. First, second and third harmonics shown.

References

- [1] H. B. Bingham, A. P. Engsig-Karup, and O. Lindberg. A high-order finite difference method for nonlinear wave-structure interaction. In *22nd Intl. Wrkshp. Water Waves and Floating Bodies*, Croatia, 2007.
- [2] H. B. Bingham and H. Zhang. On the accuracy of finite difference solutions for nonlinear water waves. *J. Engineering Math.*, 58:211–228, 2007.
- [3] R. K. C. Chan. Finite-difference simulation of the planar motion of a ship. In *Proc. 1st Intl. conf. Num. Ship Hydro.*, U.C. Berkeley Univ. Ext. Publ, 1975.
- [4] A. P. Engsig-Karup, H. B. Bingham, and O. Lindberg. An efficient flexible-order model for 3D nonlinear water waves. (Submitted), 2008.
- [5] H. J. Haussling and R. T. Van Eseltine. Finite-difference methods for transient potential flows with free surfaces. In *Proc. 1st Intl. conf. Num. Ship Hydro.*, U.C. Berkeley Univ. Ext. Publ., 1975.
- [6] R. W. Whalin. The limit of applicability of linear wave refraction theory in a convergence zone. Technical Report Res. Rep. H-71, U.S. Army Corps of Engineers, Waterways Expt. Station, Vicksburg, MS, U.S.A., 1971.